Atomic scale study of the oxygen annealing effect on piezoelectricity enhancement of (K,Na)NbO_3 nanorods

Luying Li,*[a] Xiaokang Hu,[a] Lei Jin,[b] Yahua He,[c] Shuangfeng Jia,[d] Huaping Sheng,[d] Yongfa Cheng,[a] Li Li,[a] Zhao Wang,*[e] Haoshuang Gu,[e] Yinlian Zhu,[f] Jianbo Wang[d] and Yihua Gao[a]

a. Center for Nanoscale Characterization and Devices (CNCD), Wuhan National Laboratory for Optoelectronics (WNLO), Huazhong University of Science and Technology (HUST), Wuhan 430074, P. R. China. E-mail: luying.li@hust.edu.cn

b. Ernst Ruska-Centre for Microscopy and Spectroscopy with Electrons (ER-C), Forschungszentrum Jülich GmbH, 52428, Jülich, Germany.

c. Institute for Superconducting and Electronic Materials, Australian Institute for Innovative Materials, University of Wollongong, Wollongong, New South Wales 2500, Australia.

d. School of Physics and Technology, Center for Electron Microscopy, MOE Key Laboratory of Artificial Micro- and Nano-Structures, and the Institute for Advanced Studies, Wuhan University, Wuhan 430072, P.R. China.

e. Hubei Key Laboratory of Ferro-Piezoelectric Materials and Devices, Faculty of Physics & Electronic Sciences, Hubei University, Wuhan 430062, P. R. China. E-mail: wangzhao@hubu.edu.cn

f. Shenyang National Laboratory for Materials Science (SYNL), Institute of Metal Research, Chinese Academy of Science, Wenhua Road 72, Shenyang 110016, P. R. China.

With the increasing requirement of developing non-toxic piezoelectric materials, alkaline niobate-based perovskite solid (K,Na)NbO_3 (KNN) has been intensively studied. Promising piezoelectric properties are reported, which are mostly achieved by adding other elements, or simply varying the K/Na ratio. It is found that KNN nanorods grown on conductive Nb-doped $SrTiO_3$ (STO) substrates show enhanced piezoelectric properties after annealing at 800 ^{o}C for 12 h [*Appl. Phys. Lett*. **2017**, *110*, 212904]. However, the underlying mechanism for property enhancement at the atomic scale is not clearly revealed. In this study, comprehensive transmission electron microscopy techniques are utilized focusing on the atomic scale study of the interfacial composition, structures, strain, dipolar displacement vectors and their variations along the interface normal of the as-grown and annealed KNN nanorods. The results indicate phase transformation during annealing, and a larger spontaneous polarization within each unit cell of the annealed KNN nanorods, which lead to an overall enhancement of the piezoelectric properties. These results would be very beneficial for advanced nanogenerators and sensors with enhanced piezoelectric properties.

Introduction

The direct conversion between mechanical and electrical energy with high performances has made piezoelectric materials one of the most promising candidates as energy-harvesting devices, transistors, nanogenerators, *etc*.[1-4] While $Pb(Zr,Ti)O_3$ (PZT) exhibits perfect piezoelectric properties and high Curie temperature (T_C),[5-6] the highly toxic nature of the lead composition would do harm to human body and our sustainable environment. Thus, the development of lead-free piezoelectric materials has become an urgent task.

In 2004, Satio *et al*. reported an alkaline niobate-based perovskite solid $(K,Na)NbO_3$ (KNN) modified by Li, Ta and Sb with morphotropic phase boundary (MPB), which achieved a giant piezoelectric coefficient value of 416 pC/N (d_{33}).[7] Since then, the construction of phase boundaries around room temperature through composition modification is extensively utilized for piezoelectric enhancement of lead-free piezoelectric materials. For instance, with the construction of a new rhombohedral-tetragonal (R-T) phase boundary through composition optimization, large d_{33} of ~ 490 pC/N and high T_C of ~ 304 ^oC are realized.[8] Further improved piezoelectric properties (~ 525 pC/N) are reported to be attributed to the formation of hierarchical nanodomain architectures.[9-10] In addition, the tailoring of K/Na ratio can also lead to enhanced piezoelectric properties.[11-12] It is found that the K/Na ratio of ~ 1.0 is closely related to the high piezoelectric properties of KNN ceramics.[12-14].

The relatively high piezoelectric constant of KNN, together with the special morphologies of one-dimensional KNN nanomaterials enable fabrication of piezoelectric nanogenerators and sensors of refined sizes and superior properties.[15-17] It is found that the KNN nanorod arrays grown on $SrTiO_3$ (STO) substrates show greatly enhanced performance after being annealed in oxygen at 800 ^oC, with d_{33} increasing from 140 pm/V to 360 pm/V. The observed enhancement is mainly attributed to the presence of orthorhombic-tetragonal (O-T) phase boundaries and the passivation of surface oxygen vacancies.[18] While the assumptions are mostly based on characterizations over large areas, study of the lattice matching at the KNN/STO interface and its impact on the strain distribution along the growth direction, as well as quantitative determination of the atomic crystal structures and polarization fields for as-grown and annealed KNN nano-rods would certainly bring further insight into the mechanism for the property enhancement of the annealed KNN nanorods from structural perspective.

In this work, comprehensive transmission electron microscopy (TEM) techniques are utilized to characterize the chemical and structural information of KNN nanorods grown on STO substrates. While the scanning electron microscopy (SEM) image shows the overall morphology of the as-grown KNN nanorods on STO substrate, the high-resolution transmission electron microscopy (HRTEM) image and corresponding selected area electron diffraction (SAED) pattern of the interfacial region determines the relative orientations and lattice matching conditions. Further atomic-scale characterizations including energy-dispersive X-ray spectroscopy (EDS) elemental mapping, high-angle annular dark-field (HAADF) imaging and annular bright-field (ABF) imaging techniques provide accurate information about atom types and atomic column positions of the interfacial regions, which facilitate further analysis of the polarization fields of the as-grown and annealed KNN nanorods with the experimental evidence of the property enhancement of the latter from structural point of view.

Experimental

Growth and Annealing of $(K,Na)NbO_3$ Nanorods

$(K,Na)NbO_3$ (KNN) nanorod arrays were synthesized on conductive Nb-doped $SrTiO_3$ (STO) single crystalline substrates using a surfactant-free hydrothermal process. The reagents for synthesis include potassium hydroxide (KOH, > 82%), sodium hydroxide (NaOH, > 96%), niobium pentoxide (Nb_2O_5, > 99%), and 0.7 wt. % Nb-STO substrates (100). KOH and NaOH with molar ratio of 74:26 were dissolved in distilled water, forming an alkaline solution with hydroxide concentration of 8 M. For precursor preparation, 1 g of Nb_2O_5 was added into the alkaline solution and stirred for 1 h. Then, the precleaned STO substrate was immersed in the precursor, and kept 15 mm above the bottom of the autoclave, which was moved into a stainless steel container and sealed after been

filled to 80% of the full by DI water. The autoclave was kept at 190 ^{o}C for 24 h for the hydrothermal reaction. The as-grown KNN nanorods were placed in a tube furnace and annealed in the oxygen atmosphere at 800 ^{o}C for 12 h with the oxygen flux of 30 standard-state cubic centimeters per minute (SCCM).[17-18]

Structural Characterization

The morphologies of the synthesized KNN nanorods were obtained using field-emission scanning electron microscopy (FESEM, JEOL JSM7100F). The cross-sectional samples were sliced by focused ion beam (FEI Quanta 3D FEG). The high-resolution HAADF images, ABF images and EDS elementals maps were taken from a JEOL JEM-ARM200CF microscope with double spherical aberration (C_S) correctors as well as an FEI Titan G2 80-200 ChemiSTEM microscope with a probe C_S corrector. Both microscopes were operating at 200 kV.

Results and discussion

The crystal structure of $KNbO_3$ belongs to an orthorhombic system (JCPDS Card No. 32-0822) with lattice parameters of a_o = 5.695 Å, b_o = 5.721 Å, c_o = 3.973 Å, where the subscript "o" refers to orthorhombic. The introduction of a small portion of Na on the K sites could slightly change the lattice parameters, but the overall crystal symmetry is not affected. To make the following structural analysis simpler, a pseudo-cubic system is utilized, and the relationship between the two systems can be described as: $a_c = b_c = \sqrt{\boldsymbol{a_0^2} + \boldsymbol{b_0^2}} / 2 \approx 4.036$ Å and $c_c = c_o = 3.973$ Å (*i.e.*, $a_c \parallel [1\bar{1}0]_o$, $b_c \parallel [110]_o$, and $c_c \parallel c_o$, respectively). The subscript "c" denotes pseudo-cubic and will be omitted hereafter unless specifically emphasized. Since the a_o and b_o values are slightly different, this means that the angle between ***a*** and ***b*** is slightly deviating from 90^{o} for the pseudo-cubic system.

According to the SEM image in the inset of Figure 1a, the as-grown KNN nanorods are well distributed on the STO substrate with the diameters in the range of 50-200 nm. The cross-section of the nanorods (prepared from a position far away from the KNN/STO interface) is close to a rectangular shape with its normal (i.e., the growth direction) parallel to the [010] direction and the side surfaces bounded by the (100) and (001) crystal planes. This is confirmed by TEM characterizations, as presented in Fig. S1. The lattice parameters of the as-grown KNN nanorod are measured to be a = 4.062 Å and c = 4.025 Å, which are slightly larger than those of the $KNbO_3$ bulk crystals.

To obtain detailed information about the KNN nano-rod/STO substrate interface, it is necessary to prepare TEM samples along the axial direction of the specific nanorods (or the so-called cross-sectional sample with respect to the STO substrate used in Fig. 1). Since there are large spacings between those nanorods (average spacing of ~ 200 nm), the Ga ions used in the focused ion-beam (FIB) milling could inevitably destroy the bare surfaces of the nanorods. Thus, polymethyl methacrylate (PMMA) was deposited deliberately onto the nanorods prior to the milling and used as a protective coating layer.

Fig. 1a shows a low-magnification TEM image recorded along the [100] direction of the as-grown KNN nanorod including the KNN/STO interface. The interface is labeled by a black dashed line. The corresponding HRTEM image (Fig. 1b) and SAED pattern (Fig. 1c) of the interfacial region reveal a good crystal quality of the KNN nanorod, which is consistent with the results shown in Fig. S1. The SAED pattern includes obviously two sets of diffraction spots, as evidenced by the splitting of spots (e.g., see (020) spots marked by an orange box). For these spots, the one closer to the center spot (red circle) corresponds to the KNN nanorod, which is slightly elliptical due to the limited size of the nanorod along the radial direction. The other one (blue circle) is attributed to the STO substrate with slightly smaller lattice parameters as compared to KNN, as shown in the magnified orange box in Fig. 1d.

The splitting of high-index diffraction spots (*e.g.*, see (033) spot as marked by a green box) becomes more obvious along not only the [010] direction but also the [001] direction, demonstrating that the lattice strain has been at least partially released in the KNN nanorod close to the interface. Using the lattice parameter of STO as a reference, the average lattice values are obtained: $b \approx 4.082$ Å and $c \approx 3.962$ Å, for the interfacial KNN. In comparison with the c value measured from Fig. S1, it is reasonable to deduce that following the growth of nanorods the residual lattice strain is further released in the as-grown sample.

Fig. 2a shows a high-resolution HAADF image of an as-grown KNN nanorod grown on the STO substrate. The interface region is labeled by two white arrows. All atomic columns, including NbO_2, Na/K, Sr, and TiO_2, are clearly resolved. The pure oxygen columns, however, are not visible in the HAADF image. A least-squares fit to each of the atomic position using two-dimensional Gaussian profile is carried out, and the exact atomic positions are labeled by circles of respective colors. Based on the obtained coordinates of the atomic columns, the lattice parameters in the KNN nanorod region and their variations along the interface normal are measured and presented in Fig. 2b and 2c, respectively.

For KNN unit cells, while c_{KNN} is monotonically increasing with an average value of 3.930 ± 0.013 Å over the whole area, b_{KNN} is relatively constant with comparatively larger fluctuations, and the average value of b_{KNN} is 4.010 ± 0.167 Å. The relatively larger noise level for the latter could be induced by the scanning direction along the slow scanning direction. The lattice parameters for STO are also measured with average values of c_{STO} = 3.916 ± 0.003 Å, b_{STO} = 3.916 ± 0.010 Å and will be used as reference. The c/b ratios are calculated based on the above measured lattice parameters, which show $(c/b)_{KNN}$ = 0.980, $(c/b)_{STO}$ = 1.000. Since the STO substrate is thought to be cubic, and the distortion of the image is at the minimal level, it is reasonable to deduce that the unit cell of KNN is orthorhombic.[17] It is noted that the c_{KNN} value increases from ~ 3.91 Å at the interface, suggesting that the strain along the c axis due to the confinement effect of the STO substrate is gradually released during the growth. This is again consistent with our observation that the obtained c_{KNN} value here is smaller than those measured from the SAED patterns in Fig. 1c (over relatively larger area than the HAADF image in Fig. 2a) and in Fig. S1b (recorded far away from the KNN/STO interface). The strain relaxation leads to the formation of dislocations and planar defects (*e.g.*, stacking faults), which can be seen in Fig. S2.

On the other hand, morphotropic phase boundary (MPBs) of several hundred nanometers in size are reported for KNN nanorods.[19-20] There are also 60^o, 90^o, 120^o and 180^o domains reported for KNN single crystals, which are also hundreds of nanometers or even micrometers in size.[21-22] In the current case, there isn't any obvious domain structure over large areas, which could be attributed to the limited size of the KNN nanorods. However, we do find a region including 90^o domain of ~ 10 nm in size, as shown in Fig. S3. Fig. S3a is high-resolution HAADF image of the as-grown KNN nanorod, the specific region including 90^o domain is framed in a red box, and the positions for all of the atomic columns obtained through peak-finding algorithm are overlapped in Fig. S3b. Fig. S3c is corresponding map of displacement vectors: the vectors in the upper pink region are mostly facing up left, while the vectors in the lower pink region are facing down left, leading to the formation of 90^o domain. The formation of domain boundary could be a viable way of strain relaxation for the as-grown sample.

The annealed KNN nanorods have similar morphologies as the as-grown ones. However, the EDS spectra obtained on both samples show quite different K/Na ratios which are closely related to the piezoelectricity: $(K/Na)_{as\text{-}grown}$ 3.0 and $(K/Na)_{annealed} \approx 1.0$. The decreasing K/Na ratio could be attributed to the relatively easier volatilization of K element as compared to Na at elevated temperature.[23-25] As mentioned, the KNN nanorod with (K/Na) ratio close to 1 often leads to better piezoelectric properties,[12-14] which is also valid for our annealed samples.[18] Further atomic-scale composition, structure and strain analyses at the KNN/STO interfacial region of the annealed counterpart would reveal the underlying mechanism for property enhancement.

Since the lattice parameters of KNN and STO are slightly different, the strain distribution at the KNN/STO interface is expected to be closely related to local dislocations and polarization field. The

former appears at the locations where the local atomic bonds cannot bear the strain field, the latter is largely affected by the strain induced unit cell distortions. Fig. 3a is a high-resolution HAADF image of the annealed KNN nanorod on the STO substrate, and the interface is of perfect lattice matching at atomic resolution. It is well known that the HAADF intensity is proportional to the atomic number Z^2.[26] For the KNN nanorod (the upper region), the bright spots correspond to Nb, and the much weaker spots indicate K/Na atomic columns. For the STO substrate, the Sr and Ti have relatively close atomic numbers, the slightly brighter spots are Sr, and the slightly weaker ones are Ti atomic columns.

To gain further chemical information across the interface, especially the transition layers between the two materials, a composite EDS elemental map consisting of Nb, K/Na, Sr and Ti is shown in the lower right inset of Fig. 3a with the corresponding atomic model overlaid for comparison. The transition layers are labelled by several arrows, which shows slight mixing of Sr at the K/Na atomic columns for the layer labelled by the orange arrow, mixed distribution of Nb and Ti atomic columns for the layer labelled by the green arrow, and also slight mixing of K/Na at the Sr atomic columns for the layer labelled by the red arrow. Considering the tail of the STEM probe, the observed width of the transition layer could be the upper limit of the actual condition. The coexistence of Nb and Ti atoms is also reported for the interfacial monolayer of $K_{0.5}Na_{0.5}NbO_3$ thin films deposited on $SrTiO_3$,[27] where the intermixing of K/Na and Sr atoms is not obvious as in the current case.

The corresponding intensity line profile across the KNN/STO interface in the HAADF image is overlapped in pink, and each peak position is labelled by the atomic type as indicated by the EDS mapping and the atomic model. It is apparent that the intensity of the layer labelled by the orange arrow is higher than the other K/Na layers due to mixing of the Sr atoms, while the intensity of the layer labelled by the green arrow is smaller than the other Nb layers due to mixing of Ti atoms. Meanwhile, the intensity of the Sr atomic layer labelled by the red arrow is much lower than the other Sr layers due to mixing of the K/Na atoms.

Besides the above composition mixture, the interfacial strain distribution is also measured quantitatively using geometric phase analysis (GPA), which determines the displacement field of local lattice distortion with respect to the selected reference area.[28] Fig. 3b and 3c are normal strain components along the horizontal (i.e., the in-plane component ε_{xx}) and vertical (i.e., the out-of-plane component ε_{yy}) directions, respectively. The corresponding line profiles overlapped on the strain maps obtained along the vertical direction show clearly the variations of strain components going away from the interface, which are averaged over the whole horizontal width of respective strain maps. While the out-of-plane component is fluctuating around zero (Fig. 3c), the in-plane strain component shows compressive strain at the interface, which gradually approaches zero and changes to monotonically increasing tensile strain going away from the interface (Fig. 3b). This result is quite reasonable as the KNN nanorod of slightly larger unit cell would be restrained by the contacting STO substrate, and the restriction would diminish as it is further away from the interface.

Apart from those interfacial regions with perfect lattice matching, we do find regions with stand-off misfit dislocations in the vicinity of the KNN/STO interface in order to relieve the local strain. This is in contrast to the as-grown sample. Stand-off edge dislocation was first observed at the Nb-Al_2O_3 interface, where the first metal layer maintains perfect lattice matching to minimize the interface energy, and the dislocation is formed a few atomic layers away from the interface.[29] Fig. 3d shows a typical edge dislocation on the KNN side, and the extra half plane is labelled by a symbol “T”. It is apparent that the introduction of the extra half plane leads to the distortion of local lattice planes, and the corresponding strain maps are presented in Fig. 3e (ε_{xx}) and Fig. 3f (ε_{yy}). The in-plane strain component includes a sudden reversal around the dislocation core, from compressive strain to tensile strain, and gradually approaches zero. Thus, introducing dislocations is an effective way of relieving the local strain.[30]

Meanwhile, we also find anti-phase boundaries (APBs) on the KNN side, which is four-unit cells away from the KNN/STO interface, as indicated by the blue arrows in Fig. S4. It is noted that the Nb atomic layer at the APB shows a zigzag arrangement: the Nb atom between the double-layer labelled by red lines is closer to the right side, while the Nb atom between the double-layer labelled by green lines is closer to the left side. These special atomic arrangements could be another way of relieving the interfacial strain along the [001] direction, which has also been reported for Bi_2FeMnO_6 thin films epitaxially grown on $SrTiO_3$ substrate.[31] Thus, the introduction of edge dislocations and APBs close to the KNN/STO interface could lead to further relaxation of the KNN lattices.

To obtain accurate lattice parameters of the KNN nanorod after annealing, the corresponding high-resolution HAADF image of a perfect region is shown in Fig. 4a. The KNN/STO interface is also labelled by two white arrows. After the determination of position of each atomic column, the variations of c and b along the interface normal are plotted in Fig. 4b and Fig. 4c, respectively. It seems that both c_{KNN} and b_{KNN} show increasing trend going away from the interface with the average values of c_{KNN} = 3.981 ± 0.023 Å, b_{KNN} = 3.863 ± 0.044 Å, which give $(c/b)_{KNN}$ = 1.031. Thus, the b_{KNN} axis (the growth direction) is obviously shrinking, while the c_{KNN} axis (within the interface plane) is slightly increasing, which indicates phase transformation during annealing as reported in our previous work via X-ray diffraction (XRD).[18]

It is reported that the piezoelectric properties of the as-grown KNN nanorods on STO substrates are greatly enhanced after annealing in oxygen with temperatures ranging from 500 ^{o}C to 800 ^{o}C.[18] It would be inspiring to characterize the atomic scale polarization fields within the KNN nanorods before and after annealing, which would lead to further understanding of the property enhancement of the annealed counterpart. The quantitative characterization of polarization field at atomic resolution is based on the accurate determination of atomic column positions, which has been reported to be realized through negative spherical-aberration imaging[32-33] in an aberration-corrected TEM as well as aberration-corrected HAADF imaging.[34-37]

For calculation of the displacement vectors in the KNN nanorod region, the NbO_2 column in the body center is considered as the origin, and the projected equivalent center of the eight nearest K/Na atoms is calculated, whose deviation from the origin is defined as the displacement vector. Since the displacement vector is closely related to local spontaneous polarization, mapping the displacement vectors of KNN nanorods before and after annealing would be insightful for understanding the piezoelectric property enhancement. The map of displacement vectors of the as-grown sample is presented in Fig. 2a, most of the displacement vectors are pointing downwards with an average value of 14.32 pm (NbO_2 → K/Na), and the different colors indicate different ranges of the length of the displacement vector. It is apparent that the displacement vectors in the KNN nanorod region is larger than those in the STO region, and the latter should be originated from the random noise introduced during experiment.

The map of displacement vectors for the annealed KNN nanorod is overlapped in Fig. 4a, most of the vectors are pointing to the left, which could be due to the obviously shrank b_{KNN} axis of the annealed KNN nanowire as compared to the as-grown counterpart. The average value of the displacement vector is ~ 14.95 pm for each unit cell, which is marginally larger than that for as-grown KNN nanorod and larger polarization field as a result. It is important to note that in the above analysis, we only consider NbO_2, K/Na atomic columns and their relative displacements in the KNN nanorod region, all the oxygen signals are ignored since oxygen is too light to be imaged by HAADF imaging technique. However, in some cases, it is important to take the displacement between O and the other ions into account.[36] Annular-bright-field (ABF) imaging technique is developed in recent years with great capability for detecting light elements: O, Li, or even H.[38-40] Thus, the high-resolution ABF image of the annealed KNN nanorod/STO substrate is obtained and shown in Fig. S5a. The oxygen columns are clearly observable as labelled by the purple balls, which are absent in the above HAADF images.

The displacement vectors for NbO_2 → K/Na (Fig. S5b) and NbO_2 → O (Fig. S5c) are also calculated and overlapped on the original ABF image of relatively larger area. The average NbO_2 → K/Na displacement is 14.35 pm, and the average NbO_2 → O displacement is 11.33 pm, which indicates that the former (NbO_2 → K/Na) makes the main contributions to the observed piezoelectric properties. Meanwhile, the average NbO_2 → K/Na displacement obtained from ABF imaging is very close to that measured from HAADF imaging technique considering the large differences in experimental setup and the requirement of the sample. Thus, it should be reasonable to count on the measurements of displacement vectors based on the HAADF imaging for comparing the piezoelectric properties of the as-grown and annealed KNN nanorods.

As the K/Na ratio changes from 3 to 1, the (K+Na)/Nb ratio varies from 0.94 to 0.85, and the "A-site" (in ABO_3) vacancies would increase in the oxygen annealed sample, which could lead to the distortion of local lattices and variations of displacement vectors in both amplitude and direction. With reference to the displacement vector map in Fig. 4a, the distribution of the amplitude range of the displacement vectors are uniform, which might indicate that the distribution of "A-site" vacancies is uniform as well. Meanwhile, according to the atomic resolution EDS map (the inset of Fig. 3a), the intensities of K/Na atomic columns don't show any sign of ordering, which also signifies uniform distribution of A site vacancies.

On the basis of the displacement vector maps in Fig. 2a and Fig. 4a, most of the projected unit-cell spontaneous polarizations for the as-grown samples are along *b* axis, while those for the annealed sample are along *c* axis, which correspond well with those of the O phase ([110]) and T phase ([001]), respectively.[10] A schematic of the unit cells in the O and T phases using the same axes notation (pseudo-cubic coordination system) is provided in Fig. S6 based on the measured lattice parameters before and after oxygen annealing. The slight displacements of the Nb atom as compared to the projected equivalent center of the eight nearest K/Na atoms are indicated as well.

KNN single crystals with monoclinic symmetry are also reported.[25] However, in most cases, the monoclinic phase appears in the sodium-rich KNN, while our KNN samples are on the potassium-rich side.[25,41] Thus, the existence of the monoclinic phase is eliminated based on the well-established phase diagram of KNN.[42-43]

Based on the above analyses, the high-temperature annealing treatment in oxygen would lead to changes in K/Na ratio, introducing "A-site" vacancies with local lattice distortions, and released internal strain, which work together to bring about the observed phase transition and enhanced piezoelectricity enhancement.

Conclusions

In conclusion, lead-free KNN nanorods synthesized on conductive Nb-doped $SrTiO_3$ (STO) substrates through a hydrothermal process show enhanced piezoelectric properties after annealing in oxygen atmosphere at 800 ^{o}C. To find the structural basis for the mechanism of property enhancement, the KNN nanorods before and after annealing are systematically studied by comprehensive TEM techniques. The KNN nanorods grow along [010] direction, and the rectangular nanorod cross section is bounded by (010) and (001) planes. Quantitative EDS measurements show K/Na ratio of 3.0 for as-grown nanorods as compared to 1.0 for annealed ones due to obvious volatilization of K element at elevated temperature.

Detailed interfacial analyses of the annealed KNN nanorod sample reveal elemental mixing for three layers; In region of interfacial lattice matching, the in-plane strain component gradually changes from compressive strain to zero, and then tensile strain, while in specific interfacial region including a stand-off edge dislocation, the in-plane strain component shows a sudden reverse, and quickly approaches zero. It turns out that the introduction of edge dislocations and APBs could be effective ways of relaxing the interfacial strain. According to the HAADF images of the KNN/STO interface before and after annealing at atomic resolution, the $(c/b)_{KNN}$ changes from 0.980 to 1.031 for as-grown and annealed KNN nanorods, respectively, which indicates phase

transformation during the annealing process. Further measurements of the displacement vector as pointing from each NbO_2 atomic column to the projected equivalent center of the nearest K/Na atoms reveal that the average values of the displacement vectors (NbO_2 → K/Na) in each unit cell are 14.32 pm and 14.95 pm for as-grown and annealed KNN nanorods, respectively, which indicates larger spontaneous polarization in the KNN unit cell, and overall better piezoelectric properties for annealed KNN nanorods. To be on the safe side, the displacement vector for NbO_2 → O is also measured based on high-resolution ABF image, which shows much less contribution as compared to the displacement vector for NbO_2 → K/Na. Thus, the enhancement of the annealed KNN nanorods should be mainly attributed to the phase transformation and increase of the spontaneous polarization at atomic level from structural point of view. These comprehensive analyses of interfacial composition, strain distribution, unit cell distortion and variation of displacement vectors at atomic resolution would promote insightful understanding of the underlying mechanism for property enhancement of similar heterostructural ceramics.

Conflicts of interest

There are no conflicts to declare.

Acknowledgements

This work was supported by the National Natural Science Foundation of China (51871104), the Fundamental Research Funds for the Central Universities (No. 2019kfyRCPY074).

Author contributions

L.L. (Luying Li), X.H. and L.J. performed all the experiments. L.L. (Luying Li) wrote the draft of the manuscript. S.J., H.S. and Y.Z. contributed to part of the TEM characterizations. L.L. and Z.W. raised the concepts, mechanism and analysis. J.W. and Y.G. revised the manuscript. All authors including Y.H., Y.C., L.L. and H.G. discussed the manuscript.

References

1 M. Rørvik, T. Grande and M. Einarsrud, *Adv. Mater.*, 2011, **23**, 4007-4034.
2 W. Wu, X. Wen and Z. Wang, *Science*, 2013, **340**, 952-957.
3 K. Park, S. Xu, Y. Liu, G. Hwang, S. Kang, Z. Wang and K. Lee, *Nano Lett.*, 2010, **10**, 4939-4943.
4 C. Jeong, K. Park, J. Son, G. Hwang, S. Lee, D. Park, H. Lee, H. Lee, M. Byun and K. Lee, *Energy Environ. Sci.*, 2014, **7**, 4035-4043.
5 B. Jaffe, W. Cook, H. Jaffe, *Piezoeletric ceramics*, Academic, New York, USA **1971**.
6 R. Guo, L. E. Cross, S-E. Park, B. Noheda, D. E. Cox and G. Shirane, *Phys. Rev. Lett.*, 2000, **84**, 5423.
7 Y. Saito, H. Takao, T. Tani, T. Nonoyama, K. Takatori, T. Homma, T. Nagaya and M. Nakamura, *Nature*, 2004, **432**, 84-87.
8 X. Wang, J. Wu, D. Xiao, J. Zhu, X. Cheng, T. Zheng, B. Zhang, X. Lou and X. Wang, *J. Am. Chem. Soc.*, 2014, **136**, 2905-2910.
9 B. Wu, H. Wu, J. Wu, D. Xiao, J. Zhu and S. J. Pennycook, *J. Am. Chem. Soc.*, 2016, **138**, 15459-15464.
10 T. Zheng, H. Wu, Y. Yuan, X. Lv, Q. Li, T. Men, C. Zhao, D. Xiao, J. Wu, K. Wang, J. Li, Y. Gu, J. Zhu and S. J. Pennycook, *Energy Environ. Sci.*, 2017, **10**, 528-537.
11 L. Wu, J. L. Zhang, C. L. Wang and J. C. Li, *J. Appl. Phys.*, 2008, **103**, 084116.
12 J. Hao, W. Bai, B. Shen and J. Zhai, *J. Alloys Compd.*, 2012, **534**, 13-19.
13 L. Cheng, K. Wang, Q. Yu and J. Li, *J. Mater. Chem. C*, 2014, **2**, 1519-1524.
14 L. Luo, C. Chen, H. Luo, Y. Zhang, K. Zhou and D. Zhang, *CrystEngComm.*, 2015, **17**, 8710-8719.
15 Y. Xu, Q. Yu and J. Li, *J. Mater. Chem.*, 2012, **22**, 23221-23226.
16 Z. Wang, Y. Zhang, S. Yang, Y. Hu, S. Wang, H. Gu, Y. Wang, H. L. W. Chan and J. Wang, *ACS Appl. Mater. Interfaces*, 2015, **7**, 4921-4927.
17 Y. He, Z. Wang, X.Hu, Y.Cai, L. Li, Y. Gao, X. Zhang, Z. Huang, Y. Hu and H. Gu, *RSC Adv*, 2017, **7**, 16908-16915.
18 Y. He, Z. Wang, W. Jin, X. Hu, L. Li, Y. Gao, X. Zhang, H. Gu and X. Wang, *Appl. Phys. Lett.*, 2017, **110**, 212904.
19 L. Cheng, K. Wang, J. Li, Y. Liu and J. Li, *J. Mater. Chem. C*, 2014, **2**, 9091-9098.

20 X. Meng, W. Wang, H. Ke, J. Rao, D. Jia and Y. Zhou, *J. Mater. Chem. C*, 2017, **5**, 747-753.
21 A. Benčan, E. Tchernychova, M. Godec, J. Fisher and M. Kosec, *Microsc. Microanal.*, 2009, **15**, 435-440.
22 M. Bah, N. Alyabyeva, R. Retoux, F. Giovannelli, M. Zaghrioui, A. Ruyter, F. Delorme and I. Monot-Laffez, *RSC Adv.*, 2016, **6**, 49060-49067.
23 Y. Zhen and J. Li, *J. Am. Ceram. Soc.*, 2006, **89**, 3669-3675.
24 S. Zhang, H. J. Lee, C. Ma and X. Tan, *J. Am. Ceram. Soc.*, 2011, **94**, 3659-3665.
25 H. Mgbemere, G. Schneider, M. Hoelzel and M. Hinterstein, *J. Appl. Cryst.*, 2016, **49**, 891-901.
26 P. Hartel, H. Rose and C.Dinges, *Ultramicroscopy*, 1996, **63**, 93-114.
27 C. Li, L. Wang, Z. Wang, Y. Yang, W. Ren and G. Yang, *Sci. Rep.*, 2016, **6**, 37788.
28 M. J. Hÿtch, E. Snoeck and R. Kilaas, *Ultramicroscopy*, 1998, **74**, 131-146.
29 W. Mader, G. Necker, *Metal-Ceramic Interfaces*, Pergamon Press, Oxford **1990**.
30 L. Jin, X. Guo and C. L. Jia, *Ultramicroscopy*, 2013, **134**, 77-85.
31 I. MacLaren, B. Sala, S. M. L. Andersson, T. J. Pennycook, J. Xiong, Q. X. Jia, E-M. Choi and J. L. MacManus-Driscoll, *Nanoscale Res. Lett.*, 2015, **10**, 407.
32 C. Jia, S. Mi, K. Urban, I. Vrejoiu, M. Alexe and D. Hesse, *Nat. Mater.*, 2008, **7**, 57-61.
33 C. Jia, K. W. Urban, M. Alexe, D. Hesse and I. Vrejoiu, *Science*, 2011, **331**, 1420-1423.
34 R. Mishra, Y. Kim, J. Salafranca, S. K. Kim, S. H. Chang, A. Bhattacharya, D. D. Fong, S. J. Pennycook, S. T. Pantelides and A. Y. Borisevich, *Nano Lett.*, 2014, **14**, 2694-2701.
35 L. Lu, Y. Nahas, M. Liu, H. Du, Z. Jiang, S. Ren, D. Wang, L. Jin, S. Prokhorenko, C. Jia and L. Bellaiche, *Phys. Rev. Lett.*, 2018, **120**, 177601.
36 Y. Tang, Y. Zhu, X. Ma, A. Y. Borisevich, A. N. Morozovska, E. A. Eliseev, W. Wang, Y. Wang, Y. Xu, Z. Zhang and S. J. Pennycook, *Science*, 2015, **348**, 547-551.
37 L. Li, Z. Gan, M. R. McCartney, H. Liang, H. Yu, W. Yin, Y. Yan, Y. Gao, J. Wang and D. J. Smith, *Adv. Mater.*, 2014, **26**, 1052-1057.
38 P. Gao, S. Yang, R. Ishikawa, N. Li, B. Feng, A. Kumamoto, N. Shibata, P. Yu and Y. Ikuhara, *Phys. Rev. Lett.*, 2018, **120**, 267601.
39 R. Ishikawa, E. Okunishi, H. Sawada, Y. Kondo, F. Hosokawa and E. Abe, *Nat. Mater.*, 2011, **10**, 278-281.
40 Y. Sun, L. Zhao, H. Pan, X. Lu, L. Gu, Y. Hu, H. Li, M. Armand, Y. Ikuhara, L. Chen and X. Huang, *Nat. Commun.*, 2013, **4**, 1870.
41 M. Ahtee and A. M. Glazer, *Acta Cryst*. 1976, **A32**, 434-446.
42 B. Jaffe, W. Cook and H. Jaffe, Piezoelectric Ceramics, Academic, New York, 1971, pp. 185-212.
43 J. Li, K. Wang, F. Zhu, L. Cheng and F. Yao, *J. Am. Ceram. Soc.*, 2013, **96**, 3677-3696.

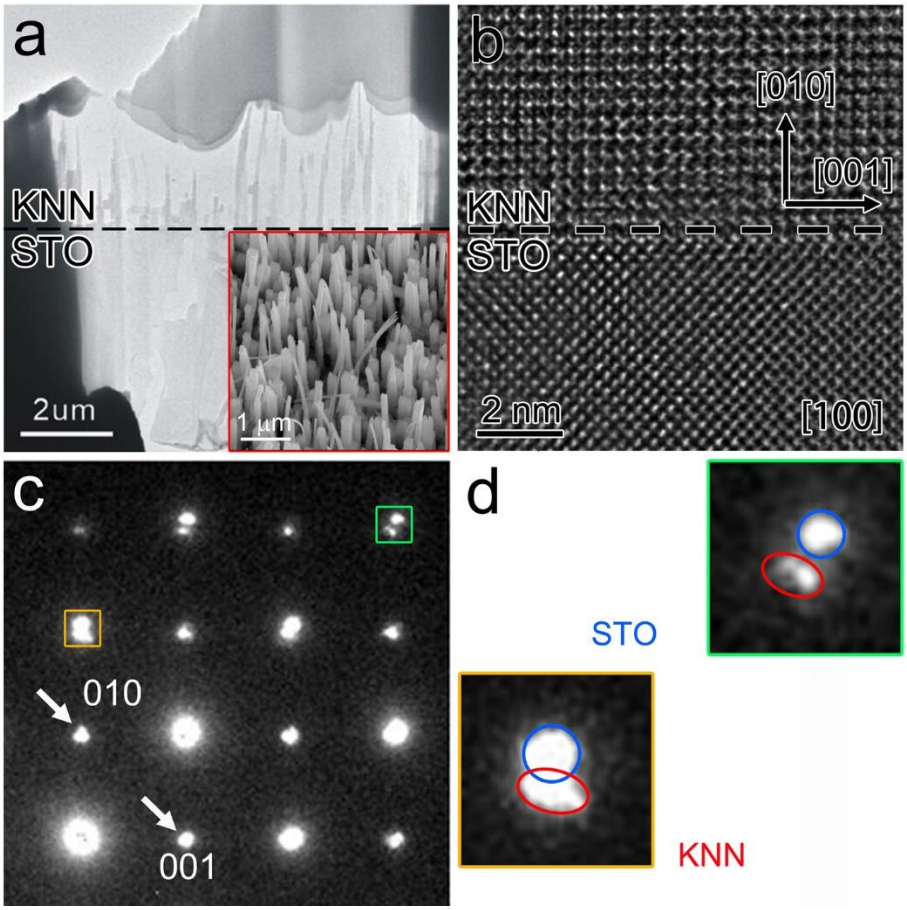

Fig. 1 Morphology and structure of the as-grown KNN/STO interface. (a) TEM image of the KNN/STO cross-sectional sample. The KNN nanorods are wrapped up by PMMA for protection during FIB thinning. The lower inset is SEM image over a large area. (b) HRTEM image of the KNN/STO interface showing single crystalline quality, the growth direction is [010], and the projection direction is [100]. (c) The first quadrant of the SAED pattern of the interfacial region with obvious splitting of certain diffraction spots. (d) The split diffraction spots as labeled by an orange box and a green box in (c) are enlarged and shown in the boxes of corresponding colors, the spots labeled by blue circles are from STO, and those labeled by red ovals correspond to KNN nanorod.

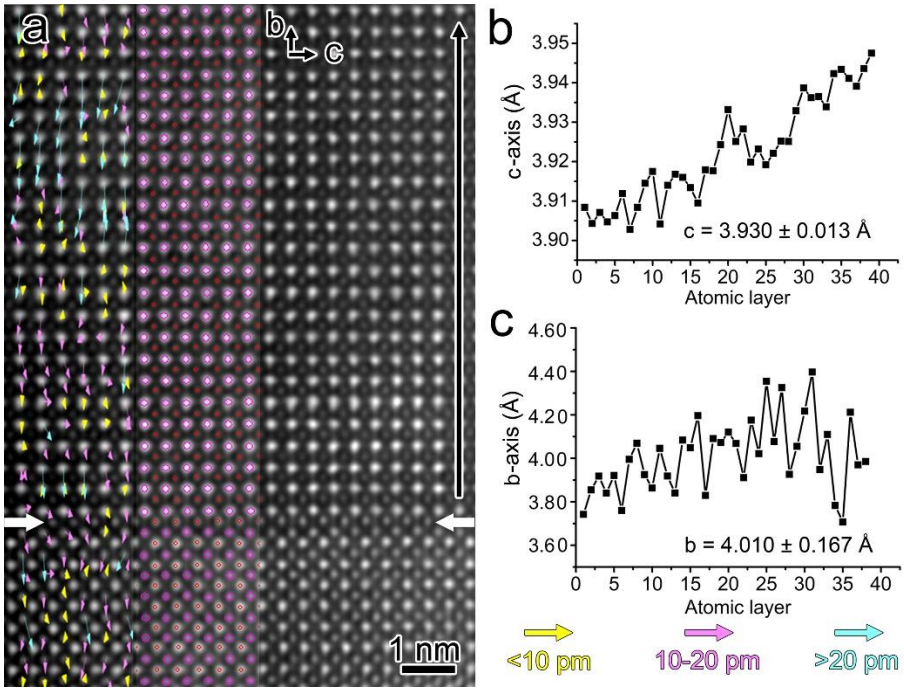

Fig. 2 Unit cell lattice parameters and displacement vectors for the as-grown KNN/STO interface. (a) High-resolution of the as-grown KNN/STO interface. The interface is labeled by two white arrows, the location of each atomic column is labeled by pink (NbO_2) and red (K/Na) circles using peak-finding algorithm. The displacement vectors (NbO_2 → K/Na) are overlapped, the different colors indicate different ranges of the length of the vector. (b) and (c) are values of *c* and *b*, and their variations along the normal direction.

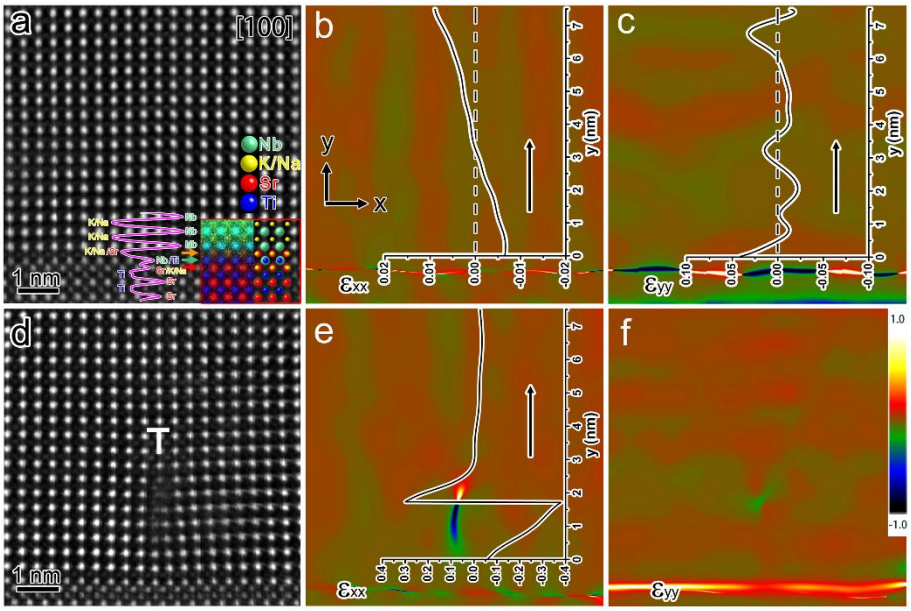

Fig. 3 Composition and strain distribution of the as-grown KNN/STO interface at atomic resolution. (a) High-resolution HAADF image of an interfacial region of perfect lattice matching. The lower inset includes EDS elemental map for each atomic column (left) and the corresponding atomic model (right). The pink curve is the intensity line profile of the HAADF image for the region under the curve. (b) and (c) are strain maps of ε_{xx} and ε_{yy} for the same region as (a), respectively. The line profiles overlapped on the strain maps are corresponding line profiles along the vertical direction for respective strain component. (d) High-resolution HAADF image of specific region including an edge dislocation. (e) and (f) are strain maps of ε_{xx} and ε_{yy} for the same region as (d), respectively. The line profile of ε_{xx} along the vertical direction is overlapped in (e). The color bar in (f) applies to all of the strain maps.

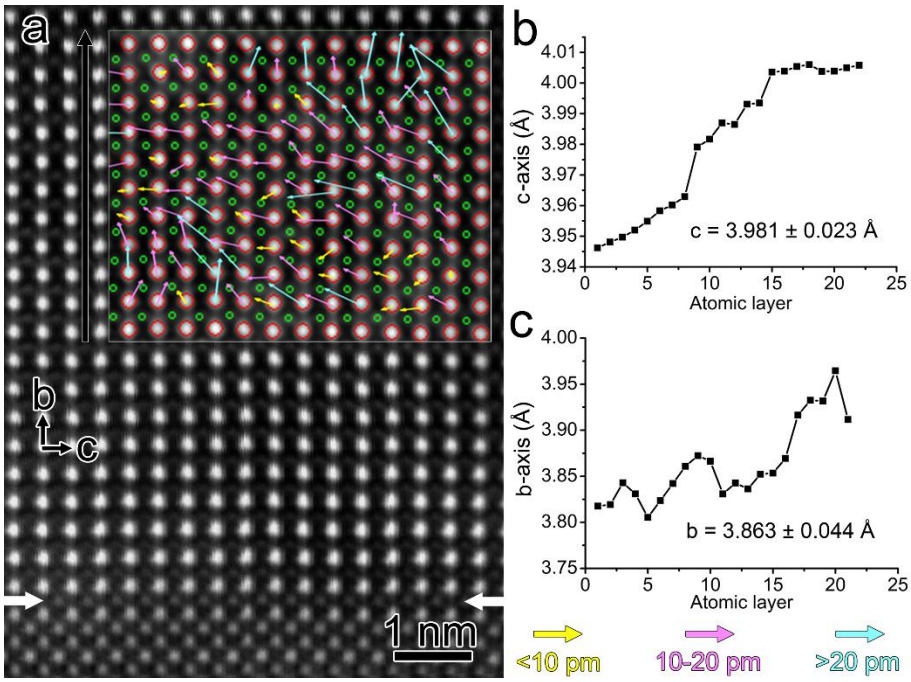

Fig. 4 Unit cell lattice parameters and displacement vectors for the annealed KNN/STO interface. (a) High-resolution of the annealed KNN/STO interface. The interface is labeled by two white arrows, the location of each atomic column is labeled by red (NbO_2) and green (K/Na) circles using peak-finding algorithm. The displacement vectors (NbO_2 → K/Na) are overlapped, the different colors indicate different ranges of the length of the vector. (b) and (c) are values of *c* and *b*, and their variations along the normal direction.